

Molecular Dynamics Simulation of Supercoiled DNA Rings

Arman Fathizadeh,^{†,‡} Helmut Schiessel,[§] and Mohammad Reza Ejtehadi^{*,||}

[†]School of Physics, Institute for Research in Fundamental Sciences (IPM), Tehran, Iran

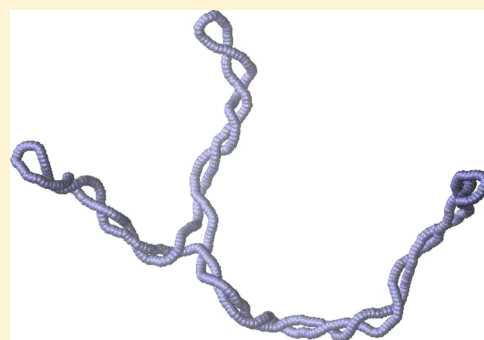
[‡]Institute for Nanoscience and Nanotechnology, Sharif University of Technology, Tehran, Iran

[§]Instituut-Lorentz for Theoretical Physics, P.O. Box 9506, 2300 RA Leiden, The Netherlands

^{||}Department of Physics, Sharif University of Technology, P.O. Box 11155-8639, Tehran, Iran

Supporting Information

ABSTRACT: DNA supercoiling is a widespread phenomenon in biology. Here we introduce a coarse-grained DNA model and study supercoiled DNA rings via a rigid body molecular dynamics simulation. Our model allows us to investigate these structures in more detail than previously. The simulations are performed on rings of one to six kilobase pairs length and are compared to available experimental data and former simulation studies. The current study provides new additional information about some of the geometrical parameters of the supercoiled DNA rings. It also shows how enforcing a supercoiled DNA ring to two-dimensional space changes its geometrical parameters. Finally, our molecular dynamics method allows us to observe some dynamical effects like the creation and movement of supercoiled branches.



I. INTRODUCTION

Mechanical properties of DNA molecules play an important role as they control their conformations and affect their functions inside cells. DNA molecules in their natural environment are typically strongly distorted away from the straight ground state, supercoiled structures being an important example. Bacterial chromosomes are typically organized into independently supercoiled loops or topological domains.¹ Small DNA rings that are overtwisting or undertwisting are another example. In the latter case, the crossing of the two DNA strands leads to a conserved integer quantity called linking number (Lk). According to the Călugareanu–White theorem^{2,3} this number is the sum of twist, Tw, and writhe, Wr: $Lk = Tw + Wr$. Supercoiling of DNA happens when the conformation of a DNA ring reduces its twist energy through writhing, thereby minimizing its total free energy.

DNA supercoiling has been studied for many years yet still remains a hot research topic.^{4–6} The available experimental data on DNA supercoiled rings mostly come from two-dimensional images of rings on a surface by electron microscopic^{7,8} or AFM images.^{5–12} However, one can expect that the conformation of the free three-dimensional supercoils can be affected by confining them on a surface. On the other hand, a lot of theoretical studies^{11,13–23} have been performed to understand the physics underlying DNA supercoiling. Those studies typically assume perfect geometries for the supercoils which may affect their predictions. Also, because of the usual DNA lengths present in the supercoiling problem, the computational simulations only have been applied in simple forms^{24–27} with less accuracy or have been applied for very short DNA lengths.^{28,29}

Here we introduce a new coarse-grained model for DNA considering one bead per six base pairs. Many simulation studies of long DNA molecules have used this resolution³⁰ or resolutions close to this,^{31–33} but most of those models fit global properties of the DNA like twisting and bending persistence length to their model. To the best of our knowledge, our model is the first coarse-grained model at this resolution which has been set up in a bottom-up scheme by two-step coarse graining of the all-atom available data on DNA. Such a model helps us to reduce the computational costs to simulate long DNA plasmids while keeping many details to obtain more information about the conformations of the supercoils. After introducing the coarse-grained model in section III. We present results of our simulation of DNA rings with different amounts of supercoiling and lengths in section IV where we also compare the results with some of the former simulation and experimental studies. We discuss two-dimensionally confined structures in section V and the diffusive motion of supercoils along the DNA rings in section VI. In section VII we present our conclusions.

II. COARSE-GRAINED MODEL FOR DNA

Several coarse-grained models have been introduced for the DNA molecule. In some cases, DNA is simply modeled as a string of beads with bonds, angles, and dihedral interacting potentials representing its stretching, bending, and twisting

Received: August 19, 2014

Revised: December 3, 2014

Published: December 18, 2014

elasticity. Recently, Brackley et al.³⁴ presented a new coarse-graining method based on discretizing the twistable wormlike chain models that gives the correct continuum limit.

Besides, a famous class of DNA coarse-grained models is the rigid base pair model in which every base pair (bp) is considered as a rigid object that only interacts with its nearest neighbors. In such models the elastic energy of a bp step can be written to first order in a harmonic form:

$$U_H = \frac{1}{2}(\psi - \psi_0)^T \cdot \mathbf{K} \cdot (\psi - \psi_0) \quad (1)$$

where ψ is a vector with six components, corresponding to the relative orientation and separation of the neighboring base pairs. The three rotational (twist, tilt, and roll) and three translational (shift, slide, and rise) parameters can be defined via several methods like the CEHS representation^{35,36} that is applied in this paper. ψ_0 represents the equilibrium configuration of the bp step, and \mathbf{K} , a 6×6 matrix, determines its stiffness coefficients. A relatively good set of these parameters was introduced by Becker et al.,^{37,38} who combined parameters obtained from protein–DNA cocrystal structures³⁶ and from all-atom molecular dynamics simulations.³⁹

In a former study⁴⁰ we have shown that this method of defining the elastic energy can be extended to higher coarse-graining levels. In this case the DNA molecule can be represented by a string of beads where each bead represents several base pairs. For such models, eq 1 can be generalized by replacing ψ_0 and \mathbf{K} with $\psi_0^{(n)}$ and $\mathbf{K}^{(n)}$, respectively, where n denotes the number of bp per bead and ψ represents step parameters between two bp that are n bp apart. Since the DNA double helix is about 2 nm thick and the separation between adjacent bp is about 0.34 nm, choosing 6 bp for coarse graining leads to an approximately spherical shape of the beads. This makes it convenient to calculate the excluded volume interactions.

To obtain $\psi_0^{(6)}$ and $\mathbf{K}^{(6)}$, we set up a Monte Carlo sampling of a 500 bp long DNA molecule. Since the effect of DNA sequence is not considered in our study, we choose in our simulation each matrix element of \mathbf{K} to be its average over of all ten possible bp steps for different sequences as given by ref 39. Furthermore, all the components of the ψ_0 are set to zero except the ones for twist, $\text{Tw}_0 = 35.0^\circ$, and rise, $\text{Ri}_0 = 3.4 \text{ \AA}$, which are set to their values for B-DNA averaged over different sequences. Using this set of parameters, we created 10 000 samples of DNA molecules from the corresponding distributions of the local bp step parameters. Calculating the step parameters for all the base pairs with six base pairs in between (which are the generalized step parameters for the higher coarse-graining level) along the DNA samples, we obtained the distributions of the generalized step parameters and, using the equipartition theorem, the corresponding generalized stiffness matrix.

Figure 1 shows the results of the Monte Carlo sampling for the distributions of the local step parameters for two neighboring bp and for two bp which are six bp apart. As can be seen, also the generalized step parameters obey a Gaussian distribution, and so it is a good approximation to use the higher level coarse graining for six base pairs. Since in the CEHS parametrization the higher level coarse-grained model has the same symmetry properties as the original rigid base pair model,⁴⁰ the average values of tilt, roll, slide, and shift for the 6 bp coarse graining are equal to zero as well. The average of the twist is simply equal to $6\text{Tw}_0 = 210^\circ$, but regarding the fact that

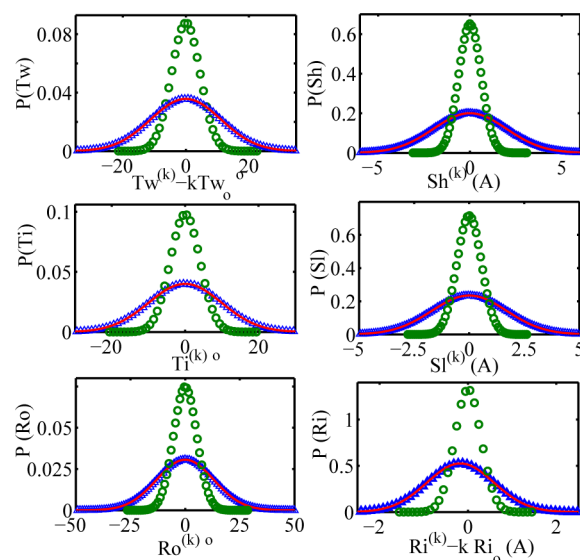


Figure 1. Distributions of the step parameters of the ordinary rigid base pair model ($k = 1$, green circles) and our generalized coarse-grained model with 6 bp units ($k = 6$, blue triangles) obtained from Monte Carlo sampling. Gaussians are fitted to the generalized step parameters (solid red line), giving an excellent description of the distributions.

the beads in the 6 bp coarse-grained model are considered to be spherical, the equilibrium value of twist can be set to zero to simplify the calculations. As can be seen in Figure 1, the expected value of the generalized rise parameter is 2.02 nm, which is a slightly smaller than $6\text{Ri}_0 = 2.04 \text{ nm}$. This reflects bending fluctuations of the 6 bp chain which shortens the rise in the same way as such fluctuation affect the end-to-end distance of semiflexible polymer chains.⁴¹ But it can be seen that in the small length scale of 6 bp this nonsymmetric effect can be neglected, and the Gaussian approximation still works well enough for the distribution of rise. The corresponding stiffness matrix, $\mathbf{K}^{(6)}$, is shown in Table 1. Our set of stiffness components leads to a DNA molecule with bending and twisting persistence lengths of about 51 and 75 nm, respectively.

Table 1. Components of the Stiffness Matrix $\mathbf{K}^{(6)a}$

	Tw	Ti	Ro	Sh	Sl	Ri
Tw	0.0100	0	0.0018	0	-0.0248	-0.0233
Ti	0	0.0102	0	-0.0027	0	0
Ro	0.0018	0	0.0062	0	-0.0018	0.0010
Sh	0	-0.0027	0	0.2528	0	0
Sl	-0.0248	0	-0.0018	0	0.4223	0.2140
Ri	-0.0233	0	0.0010	0	0.2140	1.8560

^aTranslational terms are given in units of $k_B T / \text{\AA}^2$, rotational terms in $k_B T / \text{deg}^2$, and the coupling terms between rotational and translational parameters in $k_B T / (\text{deg} \times \text{\AA})$ (k_B : Boltzmann constant; T : room temperature).

The above parametrization of DNA elasticity includes the effect of the short-ranged electrostatic interactions implicitly. What we need to add are long-ranged effects, i.e., interactions between different parts of the DNA molecule. At physiological ionic conditions the presence of small (monovalent) ions screens the electrostatic interaction to such an extent that it is a reasonable approximation to treat it like an excluded volume

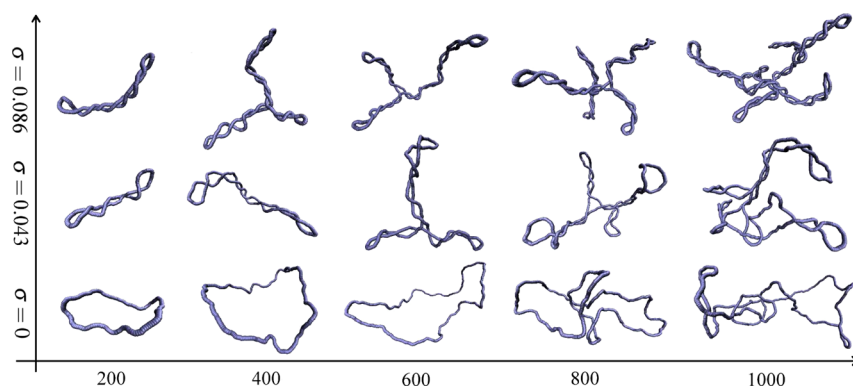


Figure 2. Snapshots of relaxed and supercoiled DNA rings for different lengths (in beads unit where every bead is equal to 2 nm) and supercoiling densities σ .

interaction. Since we chose the coarse graining such that we have spherical beads, a simple way to account for self-avoidance is to use a potential of the form of $(\lambda/r)^{12}$ where r is the center-to-center distance between beads and $\lambda = 4$ nm. Note that the hard-core diameter of the DNA double helix is about 2 nm. The larger diameter accounts for the electrostatic repulsion which is screened by salt ions. The value for λ chosen here corresponds to ionic concentrations of about 140 mM, close to physiological conditions inside a cell. Similar values have been used before (see e.g. ref 42).

III. MOLECULAR DYNAMICS SIMULATION PROCEDURE FOR SUPERCOILING

To simulate the supercoiling process, we apply a rigid body molecular dynamics simulation. The method for the extraction of forces and torques from eq 1 is explained in more detail in ref 43. The locations and orientations of the beads are updated every time step using a symplectic algorithm⁴⁴ for the integration of the equations of motions. According to the mass and size of the coarse-graining beads (6 bp), every time step in our simulations is ≈ 60 fs.

The simulations in this study are performed on rings with 200, 400, 600, 800, and 1000 beads which correspond to DNA lengths between 1.2 and 6 kbp. Initially, the beads are located on a perfect circle without any extra twist. Since the writhe vanishes for every in-plane curve, the total linking number of the ring of n beads initially depends only on its intrinsic twist, $Lk_0 = (210/360)n$. The rings are equilibrated for 50 nanoseconds (ns) in an NVT ensemble using the Nosé–Hoover chain thermostat at room temperature. To insert extra twist into the rings, our method is to reduce their intrinsic twist instead of imposing the extra twist as initial condition. This strategy allows to change the extra twist of the rings gradually which is necessary to achieve equilibrated conformations for the supercoiled DNA rings. Since the beads have spherical shapes, reducing the intrinsic twist is equivalent to increasing the extra twist. After relaxation of the DNA ring, the equilibrium value of twist changes gradually over 300 ns. This time for creating a supercoiled DNA is chosen after testing a variety of slower rates to make sure that 300 ns is slow enough for the longest DNA rings and highest supercoiling values in our simulations to avoid nonequilibrium effects. After that, the rings are equilibrated in the supercoiled state for 120 ns and then sampled for the analysis of their conformations.

IV. SIMULATION RESULTS FOR SUPERCOILED DNA RINGS

To characterize the amount of supercoiling, we use the parameter of $\sigma = \Delta Lk/Lk_0$ with ΔLk being the number of extra turns inserted into the DNA ring. The simulations are done for $\sigma = 0$, $\sigma = 0.043$, and $\sigma = 0.086$ for five different lengths. To have some statistical information about the conformations of the supercoiled rings, simulations were repeated 10 times for every length and every value of σ with different initial conditions (i.e., with different initial angular and linear velocities of the beads). In Figure 2 we present some snapshots of DNA rings from our simulation. For small lengths the rings tend to form simple supercoiled structures with two terminal loops. As can be seen by inspecting the snapshots, the number of supercoiled branches increases with increasing loop length. On the left panel of Figure 3 we show the number of superhelix

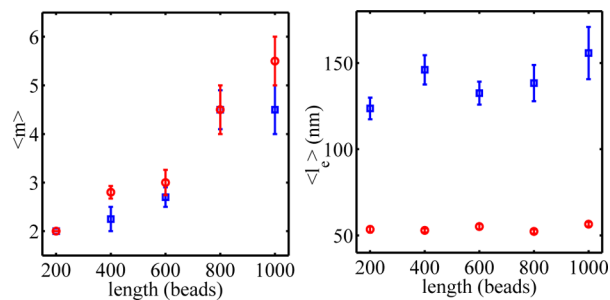


Figure 3. Average number of superhelix ends (left) and the average length of a terminal loop (right) versus ring length for $\sigma = 0.043$ (blue squares) and $\sigma = 0.086$ (red circles).

ends (terminal loops), m , averaged over 10 simulations versus DNA length for two different σ values. In most of our simulations the number of superhelix ends is constant (except for some rare cases that are shown in the section Dynamics of the Supercoils), and accordingly the m values can be easily found for each simulation through visual inspection of a few sample configurations along a simulation trajectory. We indeed find that m grows with the loop size. Also, there seems a weak dependence on σ . On the right panel the length of a terminal loop is plotted versus DNA length. This length is calculated by inspecting 100 sample configurations for each data point. The data show no significant dependence on the DNA length. This fact can be observed qualitatively in Figure 2: the typical shapes

of branched supercoils are independent of the length of the DNA rings.

In Figure 4 a supercoil is shown schematically. Indicated are two of the parameters that describe the geometry of the

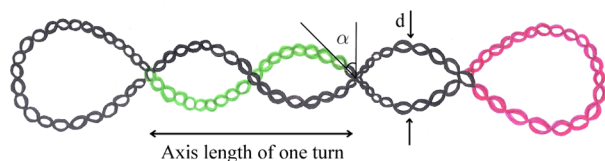


Figure 4. Schematic representation of the geometrical parameters of a DNA superhelix of diameter d and pitch angle α . A terminal loop is shown in pink and one superhelical turn in green.

supercoil, namely the diameter d and the pitch angle α . To obtain the diameter of a supercoil, we calculate the distance between all of the beads that are present in a supercoiled branch but at least 15 beads apart along the chain. This way we find a nontrivial minimum distance d_{\min} . For $\alpha > 45^\circ$ (always fulfilled in our simulation) this minimum value is equivalent to the diameter of the supercoil (see Appendix). Performing this calculation over all the beads in the ring and repeating it for enough samples over time, we obtain the probability distribution of d_{\min} shown in Figure 5 for all five lengths and

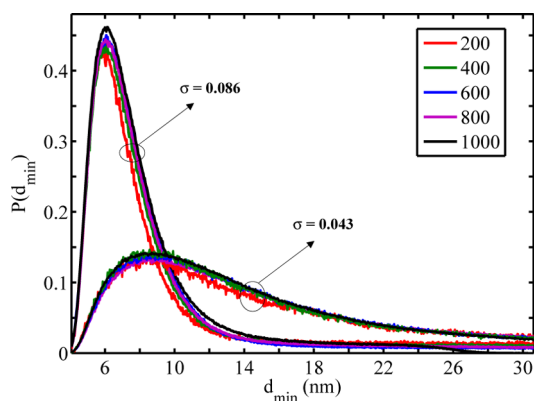


Figure 5. Probability distribution of the diameter of the supercoil for different DNA ring lengths and two values of σ : $\sigma = 0.043$ and $\sigma = 0.086$. The distributions do not depend on the DNA length but depend on the σ .

two different σ values. The self-avoiding interaction between the beads from one side and the supercoiling energy from the other side exerts limitations on the minimum distance values. This leads to a nonsymmetric distribution around a peak value. Peaks of each distribution can be considered as the diameter of the supercoil. As can be seen, the diameters of the supercoils do not depend on the length of the DNA rings which supports the qualitative results of Figure 2. Also, as it is expected, for larger values of σ the diameters of the supercoils become smaller.

Since the linking number of the ring is conserved, the total amount of writhe can be easily obtained from the value of σ and the difference in twist values before and after supercoiling, ΔTw . Figure 6 shows the average writhe values for different lengths and two different values of σ . According to this figure, writhe grows linearly with the DNA ring length. This linear behavior suggests that for this range of σ values it is possible to define a constant value for the writhe density $\rho_{wr} = Wr/l$, where l denotes the length of an arbitrary stretch of DNA. Fitting lines

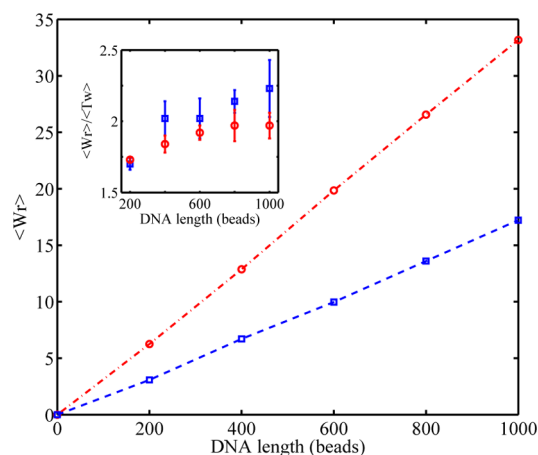


Figure 6. Average writhe values versus DNA ring length for $\sigma = 0.043$ (blue squares) and $\sigma = 0.086$ (red circles). The inset shows the ratio of average writhe to average twist as a function DNA ring length.

to the writhe curves lead to $\rho_{wr} = 0.064\sigma \text{ bp}^{-1}$. However, this value needs to be taken with caution since a constant density can only be defined for long enough pieces of DNA. Otherwise, the local writhe values would be larger near the branch ends.²⁵ The inset of Figure 6 shows the ratio of average writhe to average twist. Since the twist persistence length is larger than the bending persistence length, DNA tends to reduce its energy by transforming the extra twist to writhe. The creation of writhe costs more bending energy for short DNA rings. As the DNA ring becomes longer, writhe can be generated more easily, and the fraction of twist becomes smaller. For the rings that are long enough, the writhe-to-twist ratio saturates at a value of around 2.

To determine how the lengths of the branches are distributed, their distribution is calculated for two DNA rings with 800 and 1000 beads. Because of the low amount of branches, the available samples were not large enough to obtain the corresponding distributions for smaller ring sizes. Figure 7

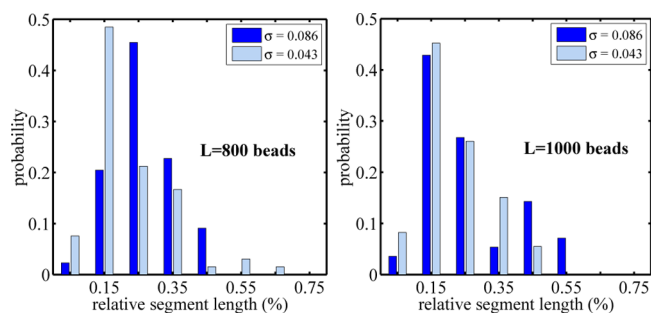


Figure 7. Distribution of the length of the branches in percentage of the total ring length for the rings with 800 and 1000 beads and for $\sigma = 0.043$ and $\sigma = 0.086$.

shows the distributions for two σ values and for the two DNA ring lengths as the percentage of the total DNA length. According to this figure, the branches are not distributed randomly in length. The peak values of the distributions suggest that branches with the length of about 15–20% of the total supercoil length are more likely to happen. The reported experimental value for a DNA ring with 7 kbp is about 10% of the total ring length.⁷ The small difference between the

experimental and simulation results might be due to the difference in ring length or the small size of available samples.

We next look at the elastic energies stored in the supercoiled rings. To find the part of the energy that is stored due to supercoiling, we subtract the energies of the supercoiled ring from its corresponding value in a relaxed ring. The resulting quantity $\Delta E_{\text{elastic}}$ is plotted separately for the twisting, bending, and the total elastic energy in Figure 8 for different ring lengths

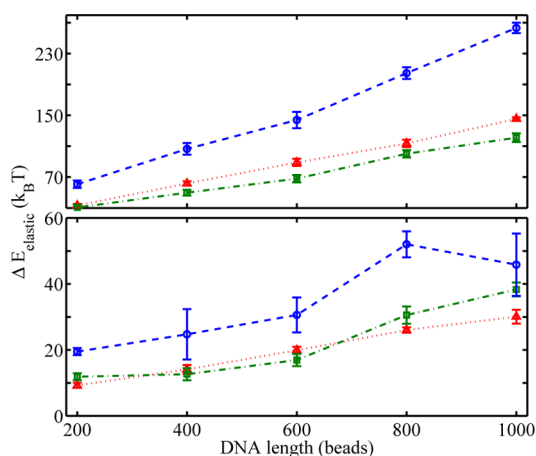


Figure 8. Total elastic energy (blue circles), bending energy (green squares), and twisting energy (red triangles) of DNA rings versus length for $\sigma = 0.043$ (bottom) and $\sigma = 0.086$ (top).

and two σ values. We collected in the twist energy the term quadratic in twist in eq 1 and half of the nondiagonal terms that couple to the twist. Similarly, the bending term contains the corresponding roll and tilt terms. First we can see from the plot that the main part of the elastic energy stems from the bending and twisting energies whereas the tensile and shear energies contribute only a tiny portion to the elastic energy. The twist energy for both σ values grows almost linearly with the ring length, which is consistent with the linear dependence of writhe with ring length (Figure 6). For $\sigma = 0.043$ the bending energy is almost the same as the twisting energy, except for the last two ring lengths. For rings with 800 and 1000 beads the number of terminal loops rises sharply as can be seen in Figure 3. The additional superhelix ends lead to an extra amount of bending energy. At higher σ values the ratio $\langle \text{Wr} \rangle / \langle \text{Tw} \rangle$ becomes smaller (see the inset in Figure 6). In fact, for $\sigma = 0.086$ the twisting energy is higher than the bending energy for all ring lengths (see top of Figure 8).

To obtain an idea how the different contributions to the elastic energy are distributed *along* a DNA ring, we show in Figure 9 a snapshot of a supercoiled ring made of 600 beads with $\sigma = 0.128$. The values of all six step parameters along the DNA rings are shown via a color scheme. It can be seen that all the parameters are randomly distributed in a uniform fashion along the ring. The roll constitutes an exception as it shows in the terminal loops large absolute values. These observations suggest that in general it is possible to define a constant line density of the different energy contributions (e.g., a twist energy density) but that one needs to be cautious with the bending energy that tends to be focused at terminal loops, an effect that becomes more important with increasing value of σ .

In addition to the above cases, we simulated the 600 beads ring for three additional σ values, $\sigma = 0.064$, 0.107, and 0.128, each repeated 10 times to obtain enough statistics. These

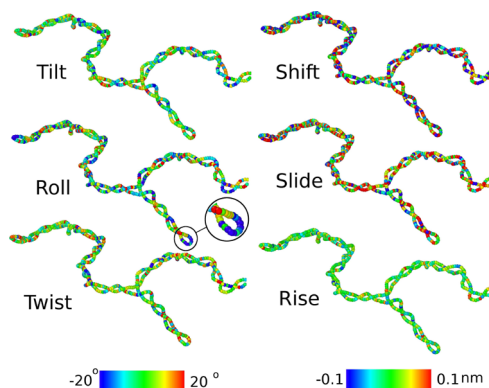


Figure 9. Distribution of the local step parameters along a supercoiled DNA ring of 600 beads with $\sigma = 0.128$. All of the parameters are distributed more or less uniformly along the DNA ring length with the exception of roll that tends to be localized in the terminal loops (see magnified portion).

simulations together with the ones from above ($\sigma = 0.043$ and 0.086) allow us to study the effect of increased supercoiling on the DNA ring conformation. Figure 10 presents the average

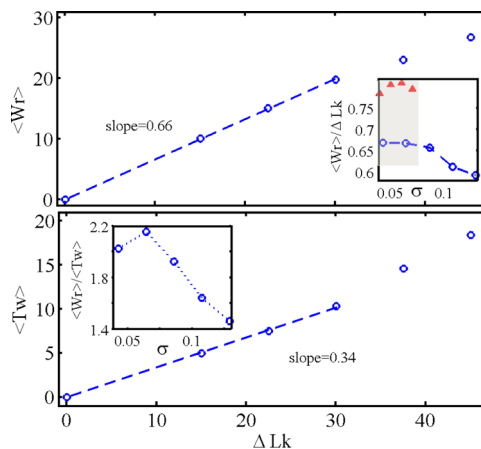


Figure 10. Average values of writhe (top) and twist (bottom) as a function of ΔLk for a ring with 600 beads. The inset in the top panel shows $\langle \text{Wr} \rangle / \Delta \text{Lk}$ versus σ . The simulation results by Vologodskii et al.²⁵ for a 3.5 kbp ring are shown as red triangles, and the shaded area indicates the range of the corresponding experimental values of Boles et al.⁷ for a 7 kbp ring. In the bottom inset the ratio of the averages of writhe and twist is plotted as a function of σ .

writhe $\langle \text{Wr} \rangle$ and the average twist $\langle \text{Tw} \rangle$ of the DNA ring as a function of ΔLk . The dashed lines are fitted to the first four points and show that both twist and writhe follow a linear behavior for smaller values of σ . The slopes of these lines (0.34 for twist and 0.66 for writhe) are close to the experimental values (0.28 for twist and 0.72 for writhe) reported by Boles et al.⁷ for a 7 kbp ring. For higher amounts of supercoiling the curves start to violate the linear behavior, and the average of twist and writhe become higher and lower than expected. This can be seen in the inset of the bottom panel of Figure 10 which shows that $\langle \text{Wr} \rangle / \langle \text{Tw} \rangle$ decreases for large σ values. This might reflect the influence of hard-core repulsion at large supercoiling values. As the chain cannot supercoil more tightly, twist cannot be transferred to writhe as efficiently. The inset of the top panel presents the results in a different way by plotting the ratio $\langle \text{Wr} \rangle / \Delta \text{Lk}$ as a function of σ . In addition, the gray shaded area

indicates the range of values found in the experiment by Boles et al.⁷ and the red triangles are the result of the Monte Carlo simulation by Vologodskii et al.²⁵ Both simulations predict values in the range of the experimental data with the former being close to the upper end whereas our results are closer to the middle.

Applying the same method explained for Figure 5, we study next the dependence of the radius of the supercoils on the value of σ . In fact, each supercoil consists of two helices wrapping around a hypothetical cylinder with its surface passing through the centers of the two DNA superhelices. The radius of this cylinder is considered as the radius of the supercoil. In Figure 11 we show the radius of the supercoil as a function of σ (blue

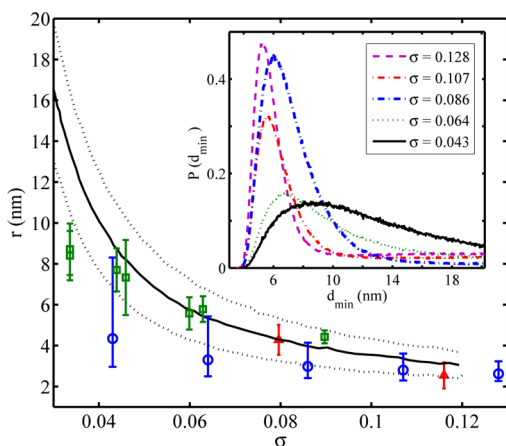


Figure 11. Supercoil radius versus σ for a DNA ring of 600 beads (corresponding to 3.6 kbp) (blue circles). For comparison, experimental results by Boles et al.⁷ (3.5 kbp (red triangles) and 7 kbp plasmid (green squares)) and a theoretical prediction¹⁷ (solid black line with the dashed line indicating the undulation amplitudes). The inset shows the corresponding distributions of the supercoil diameter for different values of σ . The supercoil radius was chosen to be half of the diameter at the peak of the corresponding distribution.

circles). The inset depicts the corresponding distributions of the supercoil diameter for each σ value. The radius of the supercoil decreases with σ . For comparison, the theoretical prediction by Odijk¹⁷ and the experimental values obtained from a 3.5 kbp supercoiled DNA by Boles et al.⁷ are shown as well. One should notice that these experimental data are obtained by analyzing two-dimensional conformations of the supercoiled DNA rings. For higher σ values the results of our simulation are consistent with both experimental data and the theoretical prediction, but for smaller σ values our simulation predicts a smaller value for the radius of the supercoil. We note, however, that the radius of the supercoil follows from the peak of the distribution and that for small σ values the distribution becomes very wide (see inset) which causes more uncertainty in the reported values. The asymmetric error bars give the radii corresponding to the half-height of the peaks and show the large uncertainty and skewness in the radii of supercoils. We further mention that both experimental and theoretical results are obtained assuming a perfect geometry for the supercoils.

To fully characterize the geometry of the supercoils, we determine in addition to their radii also the corresponding DNA length l_t of a pitch (green part in Figure 4) for various values of σ . To this end, more than 100 samples for each σ values were analyzed, and after averaging, this length l_t was calculated. Having the radii of the supercoils from Figure 11

and the values of l_t we calculated the pitch angle α from the relation⁷

$$l_t = \frac{2\pi r}{\cos \alpha} \quad (2)$$

The total axis length of the supercoiled DNA, l_a , follows approximately from the total length L , the number $\langle m \rangle$ of superhelix ends, and the geometrical parameters of the supercoil:⁷

$$l_a = \frac{\sin \alpha (L - \langle m \rangle \pi r)}{2} + \langle m \rangle r \quad (3)$$

Figure 12 shows various quantities as a function of σ . Specifically on the upper left we plot α , on the upper right the

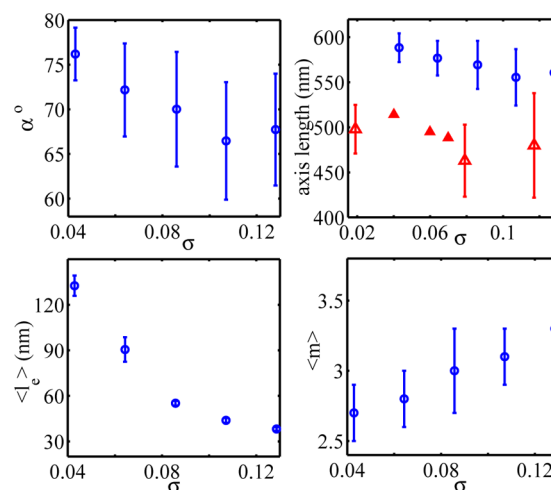


Figure 12. α (top left), average total axis length (top right), average length (bottom left), and number (bottom right) of terminal loops versus σ for a 600 beads ring. For the axis length also experimental data for 3.5 kbp plasmids (empty triangles⁷) and MC simulations (full triangles²⁵) are shown.

total axis length, on the lower left the average length of a terminal loop, and on the lower right the average number of superhelix ends. The large error bars for α do not allow us to discuss its dependence on σ . Since the values of the radii of the supercoils are smaller than the ones obtained before,^{7,25} the calculated α 's are larger than the former reported values.

Having α values, one can obtain the writhe from the perfect geometry to be equal to $n \sin \alpha$ with n being the number of nodes. For a length of l_t we have $n = 1$, and so the density of writhe over length becomes $Wr/l_t = \sin \alpha$. From the values of α and l_t for $\sigma = 0.043$ and $\sigma = 0.086$ we find writhe densities of about $0.066\sigma \text{ bp}^{-1}$, very close to the ones obtained directly from calculated writhes shown in Figure 6. For higher σ values this calculation proposes smaller writhe densities, e.g., at $\sigma = 0.128$ a writhe density of about $0.056\sigma \text{ bp}^{-1}$.

The relative axis length (upper right of Figure 12) is approximately independent of the σ . We also show experimental data (open triangles with error bars) for a 3.5 kbp DNA ring⁷ and results from Monte Carlo simulations²⁵ (full triangles). Both find slightly smaller values compared to ours, which might in part be related to the fact that the radii of our supercoils are smaller.

Finally, Figure 12 shows the sizes and numbers of the terminal loops. With increasing σ the size decreases whereas $\langle m \rangle$ seems to show a slow increase. We note that the latter

observation is not consistent with the result of former studies^{25,45} that suggest a decrease of $\langle m \rangle$ for larger σ values. This inconsistency might be due to insufficient simulation time. The computational costs do not permit us to perform micro- or millisecond simulations while it is possible that at these larger time scales some branches dissolve into each other, thereby reducing $\langle m \rangle$. If so, this process must be very slow so that is not accessible within the time scale of our MD simulations.

The elastic energies and the portions of the twist and the bending energies are shown in the top panel of Figure 13. Like

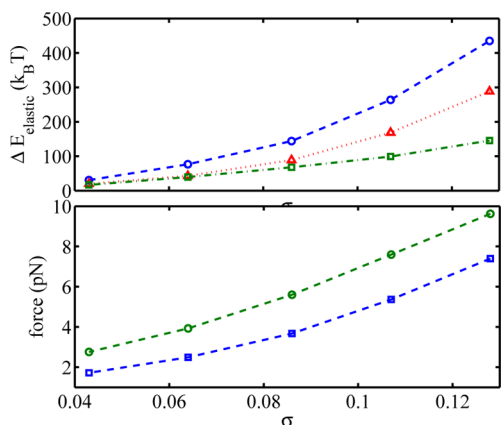


Figure 13. Top: total elastic energy (blue circles), twist energy (red triangles), and bending energy (green squares) of rings with 600 beads versus σ . Bottom: mean value of shear force (green circles) and tensile force (blue squares).

in Figure 8 the quantity $\Delta E_{\text{elastic}}$ is the difference between the energy of the supercoiled ring and a relaxed ring of the same length. The energy increases for larger σ values, and most of that increase goes into twisting energy. On the lower panel of the figure we show an estimate of the average tensile and shear forces inside the supercoiled rings. To this end, the mean values of the local step parameters of $\langle Ri - Ri_0 \rangle$, $\langle Sl \rangle$, and $\langle Sh \rangle$ were calculated and multiplied with the corresponding stiffness values. The forces also increase with σ , and the shear forces are larger than the tensile forces.

V. TWO-DIMENSIONAL STRUCTURES OF THE SUPERCOILS

In most of the experimental studies, it is necessary to deposit the DNA on a surface to observe the structure with a microscope. To mimic such conditions and study its effect on the geometrical parameters of the supercoils, we performed simulations under conditions that flatten DNA plasmids. After relaxing the DNA ring, we introduced two parallel walls with a repulsive $1/r^{12}$ potential. The walls are moved toward each other with a rate of 0.0001 Å per time step, thereby gradually confining the supercoil. We stop the process once a distance of 5 nm between the walls is reached.

Two snapshots of the confined DNA after equilibration are shown in Figure 14 for a plasmid of 600 beads: the left one for $\sigma = 0.043$ and the right one for $\sigma = 0.064$. These two values were chosen because according to Figure 11, at lower values of sigma we have the largest difference between our simulation results and the reported experimental data for the radii of the supercoils.⁷ The simulations of rings confined to two dimensions of these two sigma values give writhe values of 10.7 and 16.3, which are slightly larger than the corresponding

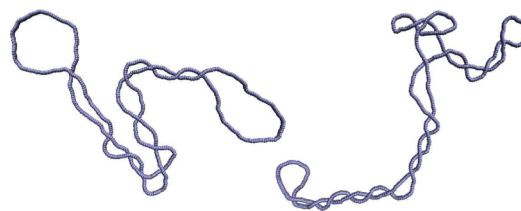


Figure 14. Snapshots of flattened supercoiled DNA rings with 600 beads for $\sigma = 0.043$ (left) and $\sigma = 0.064$ (right).

values for our free plasmids (Figure 10). The calculated slope of the curve of writhe versus ΔLk for the flattened conformations is about 0.74 (instead of 0.66, see Figure 10), which is closer to 0.72, the experimental value.⁷ We also determined in these modified simulation the supercoil radii measured parallel to the surface (i.e., as they would appear in a micrograph) and found values that are bigger than the ones we found for our free DNA rings. In summary, the results for the flattened structures suggest that some geometrical parameters change when supercoiled DNA is deposited on a surface. This could explain some of the differences between our simulations in three-dimensional space and experimental results obtained from DNA rings deposited on a surface.

VI. DYNAMICS OF THE SUPERCOILS

In most of our simulations which are performed on the scale of a hundred nanoseconds, the obtained configurations do not change significantly after the supercoiled structure has formed (for example, the number of branches stays usually constant during the course of a simulation). However, in some cases the conformations changed partly during the simulation. For instance, in Figure 15 two cases are shown in which a branch

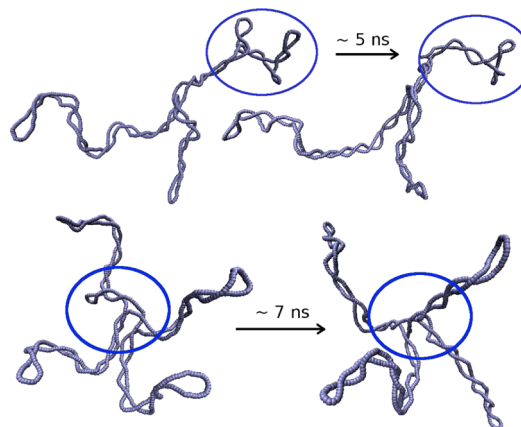


Figure 15. Two examples where branches of a supercoiled structure disappear during the time scale of nanoseconds.

disappears on a time scale of a few nanoseconds and dissolves into another branch. The geometrical values reported here are averages over enough samples. However, as mentioned before, we cannot always exclude the possibility of large scale rearrangements beyond the time scale of our simulations.

To observe whether the branches are stationary or move along the ring, we tracked the position of some tagged beads during the simulation. One typical example is shown in Figure 16 (top). In the left configuration we tag the beads at each of the three superhelix ends. After 120 ns the beads have moved substantially along the DNA ring. To obtain more information

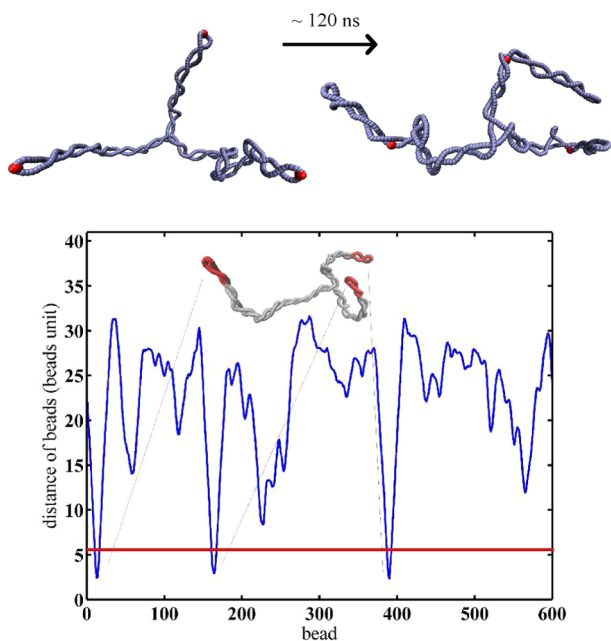


Figure 16. (top) Change in the position of the supercoils during the simulation for a ring of 600 beads and $\sigma = 0.128$. In the beginning the red beads are near tips of the supercoils, but after 120 ns they have moved to other locations. (bottom) Distance between beads that are separated by 35 beads along the ring for the depicted example configuration of a 600-bead ring at $\sigma = 0.128$. The three deep minima correspond to the 35 beads long DNA portions shown in red that are indeed located at the terminal loops. The solid red line corresponds to the threshold below which a minimum is considered to indicate a terminal loop; this threshold is set to be 2 times the diameter of the supercoil.

about dynamics, we need to define some reference points along the DNA ring. This can be done automatically for the tip of terminal loops. First, one reads off Figures 12 and 11 the typical lengths of terminal loops and diameters of supercoils for a given value of σ . Then the spatial distance between all the pairs of beads separated by the typical terminal loop length is measured. An example is shown in Figure 16 (bottom). According to this curve, one can relate the three deepest minima to those beads which are located at the terminal loops. The end-to-end distance of these minima during the simulation does not exceed twice of the supercoil diameter (red line in Figure 16). Doing the same calculation for the whole trajectory, it becomes possible to follow the motion of the loops and observe sliding motion of the base pairs along the DNA ring. Figure 17a shows such curves for trajectories of two out of the three terminal loops (inset Figure 16) in two long simulations of about 700 ns for two DNA supercoiled rings of 600 beads and for $\sigma = 0.128$ and $\sigma = 0.086$. First of all, note the interesting fact that in both cases the trajectories of the end loops are nearly parallel. This suggests that the fastest mode of rearrangement in the twisted rings is a reptation-like motion of the whole chain through a fixed overall geometry as it can also be seen directly in the example shown in Figure 16 (top). The subtraction of the two curves which belong to the same ring is equivalent to the relative motion of two branches in a ring. It is plotted in Figure 17b and confirms the slow dynamics of the overall branched geometry of the ring. Figure 17c shows the average autocorrelation of the relative motion of three branches with

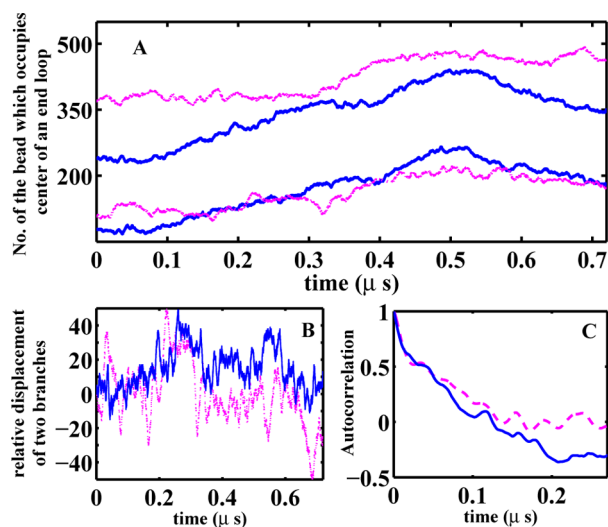


Figure 17. (A) Trajectories of the centers of two end loops (given by the corresponding bead numbers) versus time for $\sigma = 0.128$ (blue) and $\sigma = 0.086$ (pink). (B) Relative displacement of two branches in a ring which is found by subtracting position of the center of two terminal loops for $\sigma = 0.128$ (blue) and $\sigma = 0.086$ (pink). (C) Autocorrelation of the relative displacement of the branches.

respect to each other. This autocorrelation vanishes on the time scale of a few hundreds of nanoseconds.

Even though our model allows to observe some of the dynamics in the supercoils, our simulation time scale is not large enough to obtain diffusion coefficients for the motion of the branches. Finally, we stress that the observed sliding motion is energetically not costly in our DNA model as the elasticity is homogeneous along the chain. We should, however, mention that sequence-dependent DNA elasticity could lead to the pinning of supercoils in real DNA at positions where prebent or easily bendable sequences are located at the tips of the supercoils. Experiments on fluorescently labeled DNA do indeed suggest such a pinning of supercoils.⁴

VII. CONCLUSION

In this paper a generalized rigid base pair model with a 6 base pair resolution was introduced. This model was used to study the conformations of supercoiled DNA rings. The results are in fair agreement with the experimental data of Boles et al.⁷ The main difference between the results of the current study and former experimental and theoretical results was in predicting the radii of the supercoils. The calculated values from our simulations propose smaller values for the radii of the supercoils. This inconsistency might be due to several reasons. First, the former reported values were based on considering a perfect shape for supercoils while we calculate the values from the distribution of the minimum distance between the beads. Second, we have shown that the geometrical parameters of the supercoils can be perturbed in two-dimensional space. For instance, we observed that the writhe for a supercoil confined in two-dimensional space agrees better with experimental values. Moreover, our study proposes that in two-dimensional case the average radii become larger than their values in three-dimensional space.

In addition to these geometrical parameters we obtained the phase space for DNA rings of different lengths and σ values. We mention that due to computational costs it was not possible for us to perform simulations on the micro- or millisecond time

scales; instead, simulations were only performed for 120 ns after relaxing the structures. We cannot exclude the possibility that some branches might dissolve into each other for longer simulation times. On the other hand, the molecular dynamics method helped us to directly observe some phenomena like the creation or disappearance and the movement of supercoiled branches during the limited simulation time.

Finally, it is worth mentioning that our newly introduced model for DNA simulations might be useful for the study of other problems involving DNA mechanics like DNA confinement in viral capsids.

■ APPENDIX. DIAMETER OF THE SUPERCOIL

The diameter of the supercoil is calculated based on the distribution of the minimum distance of the beads. But the minimum distance is not always equivalent to the diameter of the supercoil. Consider two helices that are wrapped around a cylinder of radius a . The equation of the supercoil can be parametrized as $(a \sin t, a \cos t, bz)$ where $\tan \alpha = b/a$. Assuming a point such as $(0, -a, 0)$ on the other helix, one can calculate the distance from this point to the first helix by taking variation from the equation

$$d^2 = 2a^2(1 + \cos t) + b^2t^2 \quad (4)$$

Taking variation from the above equation solving it to find the minimum distance leads to $\sin t = \tan \alpha^2 t$. For $\tan \alpha > 1$ the only solution is $t = 0$, which corresponds to $d = 2a$. According to Figure 12, the α is always greater than 60° , which guarantees applying minimum distance calculation for finding the supercoils diameters.

■ ASSOCIATED CONTENT

● Supporting Information

Supplementary movie shows a sample of the coarse-grained MD simulations on a DNA supercoiled ring at its equilibrated state. After 300 ns of supercoiling procedure and 100 ns of equilibration, this sample makes five supercoil branches: One web connects to 4 branches each containing one terminal loops. This material is available free of charge via the Internet at <http://pubs.acs.org>.

■ AUTHOR INFORMATION

Corresponding Author

*E-mail: ejtehadi@sharif.edu (M.R.E.).

Present Address

A.F.: Physics Department, University of Illinois at Chicago, Chicago, IL 60607.

Notes

The authors declare no competing financial interest.

■ ACKNOWLEDGMENTS

We thank Hossein Salari and Hamid Seyyed Allaei for helpful discussions.

■ REFERENCES

- (1) Postow, L.; Hardy, C. D.; Arsuaga, J.; Cozzarelli, N. R. *Genes Dev.* **2004**, *18*, 1766–1779.
- (2) Călugareanu, G. *Rev. Math. Pures Appl.* **1959**, *4*, 5–20.
- (3) White, J. H. *Am. J. Math.* **1969**, *91*, 693–728.
- (4) van Loenhout, M.; de Grunt, M.; Dekker, C. *Science* **2012**, *338*, 94–97.

- (5) Schmatko, T.; Muller, P.; Maaloum, M. *Soft Matter* **2014**, *10*, 2520–2529.
- (6) Meng, H.; Bosman, J.; van der Heijden, T.; van Noort, J. *Biophys. J.* **2014**, *106*, 1174–1181.
- (7) Boles, T. C.; White, J. H.; Cozzarelli, N. R. *J. Mol. Biol.* **1990**, *213*, 931–951.
- (8) Cherny, D. I.; Jovin, T. M. *J. Mol. Biol.* **2001**, *313*, 295–307.
- (9) Bustamante, C.; Vesenka, J.; Tang, C. L.; Rees, W.; Guthold, M.; Keller, R. *Biochemistry* **1992**, *31*, 22–26.
- (10) Lyubchenko, Y. L.; Shlyakhtenko, L. S. *Proc. Natl. Acad. Sci. U. S. A.* **1997**, *94*, 496–501.
- (11) Lee, N.-K.; Schmatko, T.; Muller, P.; Maaloum, M.; Johnner, A. *Phys. Rev. E* **2012**, *85*, 051804.
- (12) Billingsley, D. J.; Kirkham, J.; Bonass, W. A.; Thomson, N. H. *Phys. Chem. Chem. Phys.* **2010**, *12*, 14727–14734.
- (13) Hao, M. H.; Olson, W. K. *Macromolecules* **1989**, *22*, 3292–3303.
- (14) Marko, J. F.; Siggia, E. D. *Science* **1994**, *265*, 506–508.
- (15) Marko, J.; Siggia, E. *Phys. Rev. E* **1995**, *52*, 2912.
- (16) Strick, T.; Allemand, J.-F.; Bensimon, D.; Bensimon, A.; Croquette, V. *Science* **1996**, *271*, 1835–1837.
- (17) Ubbink, J.; Odijk, T. *Biophys. J.* **1999**, *76*, 2502–2519.
- (18) Bouchiat, C.; Mezard, M. *Phys. Rev. Lett.* **1998**, *80*, 1556.
- (19) Bouchiat, C.; Mezard, M. *Eur. Phys. J. E* **2000**, *2*, 377–402.
- (20) Neukirch, S.; Marko, J. *Phys. Rev. Lett.* **2011**, *106*, 138104–1–4.
- (21) Clauvelin, N.; Audoly, B.; Neukirch, S. *Macromolecules* **2008**, *41*, 4479–4483.
- (22) Emanuel, M.; Lanzani, G.; Schiessel, H. *Phys. Rev. E* **2013**, *88*, 022706.
- (23) Marko, J.; Neukirch, S. *Phys. Rev. E* **2013**, *88*, 062722–1–18.
- (24) Klenin, K. V.; Vologodskii, A. V.; Anshelevich, V. V.; Dykhne, A. M.; Frank-Kamenetskii, M. D. *J. Mol. Biol.* **1991**, *217*, 413–419.
- (25) Vologodskii, A. V.; Levene, S. D.; Klenin, K. V.; Frank-Kamenetskii, M.; Cozzarelli, N. R. *J. Mol. Biol.* **1992**, *227*, 1224–1243.
- (26) Sprou, D.; Harvey, S. C. *Biophys. J.* **1996**, *70*, 1893–1908.
- (27) Chirico, G.; Langowski, J. *Biopolymers* **1994**, *34*, 415–433.
- (28) Lankaš, F.; Lavery, R.; Maddocks, J. *Structure* **2006**, *14*, 1527–1534.
- (29) Mitchell, J. S.; Harris, S. A. *Phys. Rev. Lett.* **2013**, *110*, 148105.
- (30) Rollins, G. C.; Petrov, A. S.; Harvey, S. C. *Biophys. J.* **2008**, *94*, L38–L40.
- (31) Marenduzzo, D.; et al. *Proc. Natl. Acad. Sci. U. S. A.* **2009**, *106*, 22269–22274.
- (32) LaMarque, J. C.; Le, T.-v. L.; Harvey, S. C. *Biopolymers* **2004**, *73*, 348–355.
- (33) Petrov, A. S.; Harvey, S. C. *Biophys. J.* **2008**, *95*, 497–502.
- (34) Brackley, C.; Morozov, A. N.; Marenduzzo, D. *J. Chem. Phys.* **2014**, *140*, 135103.
- (35) El Hassan, M.; Calladine, C. *J. Mol. Biol.* **1995**, *251*, 648–664.
- (36) Olson, W. K.; Bansal, M.; Burley, S. K.; Dickerson, R. E.; Gerstein, M. *J. Mol. Biol.* **2001**, *313*, 229–237.
- (37) Becker, N.; Wolff, L.; Everaers, R. *Nucleic Acids Res.* **2006**, *34* (19), 5638–5649.
- (38) Becker, N.; Everaers, R. *Phys. Rev. E* **2007**, *76*, 021923.
- (39) Lankas, F.; Sponer, P.; Langowski, J.; Cheatham, T. E. *Biophys. J.* **2003**, *85*, 2872–2883.
- (40) Fathizadeh, A.; Eslami-Mossallam, B.; Ejtehadi, M. *Phys. Rev. E* **2012**, *86*, 051907.
- (41) Rubinstein, M.; Colby, R. H. *Polymer Physics*; Oxford University Press: Oxford, 2003.
- (42) Marko, J. F.; Siggia, E. D. *Science* **1994**, *265*, 506–508.
- (43) Fathizadeh, A.; Besya, A. B.; Ejtehadi, M. R.; Schiessel, H. *Eur. Phys. J. E* **2013**, *36*, 21–1–10.
- (44) Kamberaj, H.; Low, R. J.; Neal, M. P. *J. Chem. Phys.* **2005**, *122*, 1906216.
- (45) Marko, J. F.; Siggia, E. D. *Phys. Rev. E* **1994**, *52*, 2912–2938.